Asian Journal of Chemistry; Vol. 30, No. 12 (2018), 2737-2742

ASIAN JOURNAL OF CHEMISTRY

https://doi.org/10.14233/ajchem.2018.21574

Carbon Monoxide Gas Sensor Based on Fe-ZnO Thin Film

PUSHPENDRA KUMAR*, SAMIKSHA, SHALINI and RUBY GILL

Department of Chemistry, Lovely Professional University, Phagwara-144 411, India

*Corresponding author: E-mail: pushpendra.kmr1@gmail.com

Received: 12 July 2018; *Accepted*: 20 September 2018; *Published online*: 31 October 2018; AJC-19140

In this study, we have investigated the sensing properties of ZnO and Fe-ZnO thin films synthesized by sol-gel spin coating method over transparent conducting glass. The films were subjected to XRD, UV-visible spectroscopy for phase, microstructural and optical properties which confirm the exhaustive evolution of hexagonal wurtzite phase having band gap in UV range. The morphological and topological properties were investigated by SEM and AFM. The sensing properties of ZnO and Fe-ZnO were investigated by using them as an electrode material and recording their resistance in air and in presence of CO gas. Fe-ZnO thin film was found to be more sensitive compared to ZnO thin films having good stability over the days.

Keywords: Fe-ZnO thin films, CO sensors.

INTRODUCTION

Overutilization of transport and rapid industrial development is leading to highly distortive air quality. To avoid this, regular monitoring of air polluting gases is required. Over the conventional methods like liquid chromatography or gas chromatography, a new highly sensitive, efficient and low cost device is required. Now a days various gas sensors are available but reductive gas sensor based on metal oxides are attracting a lot of attention due to low cost, high sensitivity, easy fabrication, easy modification at molecular level and compatibility with electrical devices [1]. Out of various semiconductor system, ZnO has emerged as a favourite candidate for sensing use as it possess high electrical mobility, stability, low toxicity and good oxidation resistibility [2]. The sensitivity is based on the change of conductance/resistance when any gas undergoes chemisorption on ZnO surface. Here the selectivity of the gas is a key point. The sensors having high sensitivity have been developed but selectivity is still a matter of concern. Selectivity means the response produced by a sensor for a particular gas compared to other gases [3]. The selectivity of normal ZnO is not good as surface states of ZnO can be changed by many types of gas and thus produce similar kind of response [3]. This limitation can be overcome by the modification of chemisorption by changing the surface properties. Other important property of gas sensor is operating temperature. Most of the sensors are affective at higher operating temperature which may cause problem especially with flammable gases. Many strategic tools have been adopted to modify the material properties to improve selectivity and sensitivity such as doping, heterostructures, fabricated nanoarchitectures [4-6].

Doping is one of the best ways to tailor out any material as it does not only induce intra band gap states but also modify the electrical, optical properties and microstructural properties. The change in conductivity on exposure of sensor to gas is a key factor determining its efficiency, depending on porosity, surface morphology and band gap energy [7]. By doping with suitable dopant the sensitivity as well as gas selectivity of sensor may be enhanced [4]. Surface to volume ratio which is very important parameter for sensing can be altered by doping. However, the selectivity of dopant is important. It should not cause enough strain in the host crystal lattice leading to the distortion of crystal lattice.

To enhance the efficiency of the sensing material, nanotechnology can be used as tailoring tool to modify the favourable properties pertaining to the sensitivity [8]. Different nanostructures of ZnO have been investigated due to its various favourable properties such as electrical, structural, optical and morphological properties [9]. Metal oxides nanostructures offer high surface to volume ratio and porosity which is very

important for chemisorption of any gas. In this study, Fe doped ZnO thin films were synthesized and were used as sensor for carbon monoxide gas sensor at different operating temperature.

EXPERIMENTAL

To synthesize the ZnO thin films, zinc acetate dihydrate ($ZnOAc{\cdot}H_2O$) was used as a starting material. The selection of precursor salt was based on the fact that hydrolysis product of acetate group are soluble in solvent and can be easily decomposed into volatile compounds. A colloidal gel was prepared by refluxing zinc acetate dihydrate in ethanol for 4 h at 70 °C. Appropriate amount of diethanolamine was added as stabilizer. As synthesized precursor solution was kept for 24 h for aging and stabilization. The film was deposited by spin coating method at 2000 rpm. After each deposition, samples were placed on hot plate so as the excess of solvent can be vapourized. Condensation reaction followed by solvent evaporation resulted deposition of solid film on substrate. Finally films were annealed at 600 °C followed by preheating at 250 °C. For Fe doping iron nitrate was added along with zinc acetate and then similar method was followed.

As synthesized films were subjected to X-ray diffraction analysis for phase and crystalline size analysis (Bruker AXS D8 Advance, Germany). Scherrer's calculations were attempted to estimate average grain size in the samples. Absorption curves of ZnO and Fe doped ZnO films were recorded by employing double beam UV-visible spectrophotometer (UV-1800, Shimadzu). Morphological study was done by scanning electron microscopy (SEM) using Zeiss Ultra 55-Limited edition scanning electron microscope while topological investigation was done by using AFM (Nanosurfeasyscan, Switzerland). The sensor response was recorded in presence of CO and in air (used as reference). Resistance of ZnO and Fe doped ZnO thin films of dimension 1 cm × 1 cm was recorded in air and then after injection of target gas in air tight chamber of steel. The sensor response was evaluated by using a formula, $S = R_a/R_g$, where R_a and R_g are the resistance in air and gas, respectively. Electrical resistance was recorded at different temperature by using two probe method.

RESULTS AND DISCUSSION

In the present work, ZnO and Fe doped ZnO thin films were prepared by sol-gel spin coating method. Zinc acetate dihydrate was used as the source of Zn^{2+}. Zinc acetate avoids the penetration of large amounts of solvent to the sol-gel and thereby enabling the control over reactions occurring within the sol-gel. In sol-gel preparation, after deposition, colloidal polymer supported by long chain organic molecules is formed [10]. During annealing metal ions detach from the organic chain and form primary oxide crystallites. The transition temperature at which ZnO starts to form is 240 °C [11]. The films were annealed at 600 °C so that proper crystallization can be take place. The observed density of ZnO and Fe doped ZnO were found to be 5.08 and 4.93 g cm^{-3}, respectively, which is lower than theoretical density (5.60 g cm^{-3}) indicating that films are highly porous.

Fig. 1 depicts the observed X-ray diffraction pattern of ZnO and Fe doped ZnO thin films and shows the exhaustive evolution of hexagonal wurtzite phase of ZnO. The peaks at 2θ 31.7, 34.5, 36.2, 47.6 and 56.7 corresponding to planes (100), (002), (101), (102), (110) respectively, confirms the hexagonal wurtzite phase of ZnO. Other high intensity peaks at 2θ 26.5, 33.8, 37.8, 51.7 and 54.7 can be attributed to the underlying SnO_2: F layer on the substrate. Another peaks of very low intensity were also observed at 35.40 and 53.75 corresponding to $ZnFe_2O_4$. No peak corresponding to Fe_2O_3 was observed indicating a proper doping of Fe in ZnO crystal lattice. The ionic radii of Zn^{2+} is 0.74 nm and is quite comparable to that of Fe^{3+} which is 0.68 nm [12]. As ionic radii of Zn^{2+} is slightly larger than Fe^{3+}, a proper incorporation in the ZnO lattice is expected and no separate phase of iron or iron oxide was observed in X-ray diffraction pattern. However, on incorporating of Fe, the peak intensity decreased which indicates the reduction in crystallinity. As any foreign chemical species is introduced to crystal lattice, depending upon the ionic radii there may be contraction or expansion to accommodate the foreign moiety which causes strain and stress in crystal lattice resulting in lower crystallinity [13]. XRD data was utilized to calculate crystalline size. The crystalline size of pure ZnO thin film was found to be 37 nm which reduced to 29 nm on Fe doping. Table-1 depicts the microstructural parameters calculated by XRD data. The lattice parameters 'a' and 'c' were also calculated and it was found that lattice parameters increased on Fe doping compared to undoped ZnO. This increase in lattice parameter may be attributed to the opening of crystal lattice to accommodate foreign moieties. This opening in crystal lattice may induce the strain and can cause reduction in crystal quality and we observed the same as crystalline size decreased on Fe doping. XRD data was also utilized to evaluate microstrain and dislocation density. The observed microstrain was increased from 0.9×10^{-3} to 1.19×10^{-3} on Fe doping. It is known that due to strain peak shift either towards lower angle or higher angle depending upon the ionic radii. In Fig. 2, a slight right shift in diffraction peaks were observed in Fe doped

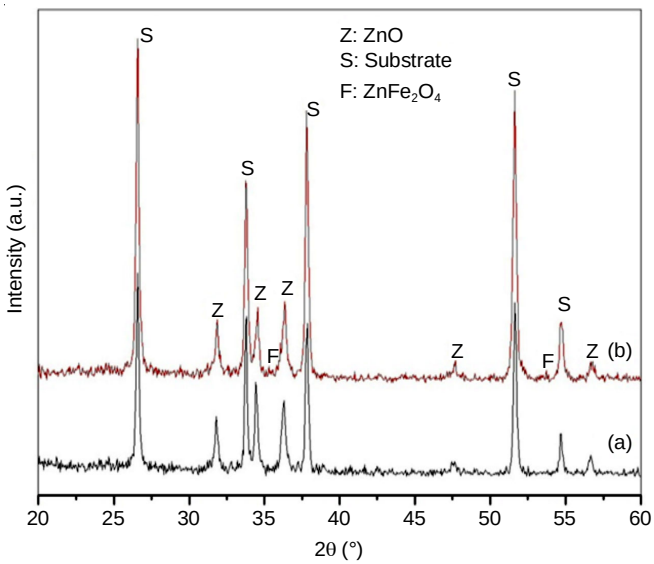

Fig. 1. X-ray diffraction pattern (a) undoped ZnO (b) Fe doped ZnO thin films

TABLE-1

Parameters	ZnO	Fe-ZnO
Crystalline size	37	29
d	2.60192	2.63503
a	3.186	3.227
c	5.203	5.270
Bond length	1.961 Å	1.977 Å
Dislocation density ($\times 10^{-14}$) nm^{-2}	7.30	11.89
Microstrain	0.9×10^{-3}	1.19×10^{-3}
Band gap	3.24 eV	2.93 eV

ZnO. The shifting of peaks towards higher angle indicates the presence of Fe^{3+} as the ionic radii of Fe^{3+} is smaller than that of Zn^{2+} [14].

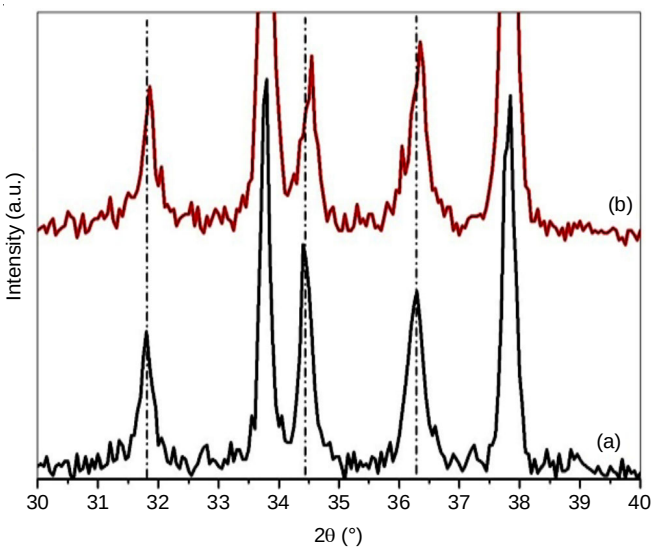

Fig. 2. Shifting of peaks on Fe doping (a) undoped ZnO (b) Fe doped ZnO thin films

The optical properties were analyzed by UV-visible spectroscopy. Fig. 3 shows the absorption spectra of ZnO and Fe- ZnO thin films, which shows strong optical absorption in UV region. However, on doping absorption shifted towards longer wavelength. This shift can be attributed to Fe doping as doping may induce intra band gap states. In case of Fe doped ZnO, the relative absorption was also increased which can be attributed to *d-d* transitions of Fe ions [15]. The absorption data was utilized to evaluate band gap and it was observed that on Fe doping band gap reduced from 3.24 to 2.93 eV (Fig. 4).

Fig. 5 shows the AFM images of pure ZnO and Fe doped ZnO thin films. In both the cases film deposition was almost uniform without any major structural defect or pin holes. Well-formed crystals with clear grain boundaries can be seen. The 3D AFM images reveal that the crystal growth is perpendicular to the substrate which is also confirmed by XRD as intense peak corresponding to (002) plane was observed. Crystalline growth perpendicular to the substrate offer more surface area for the reaction and is beneficial for sensing purpose. In case of Fe doped ZnO crystals are comparative have small size than that of pure ZnO and are in good agreement with XRD as crystalline size decreased on Fe doping. So AFM images reveal uniform deposition of film on the substrate having good crystalline quality.

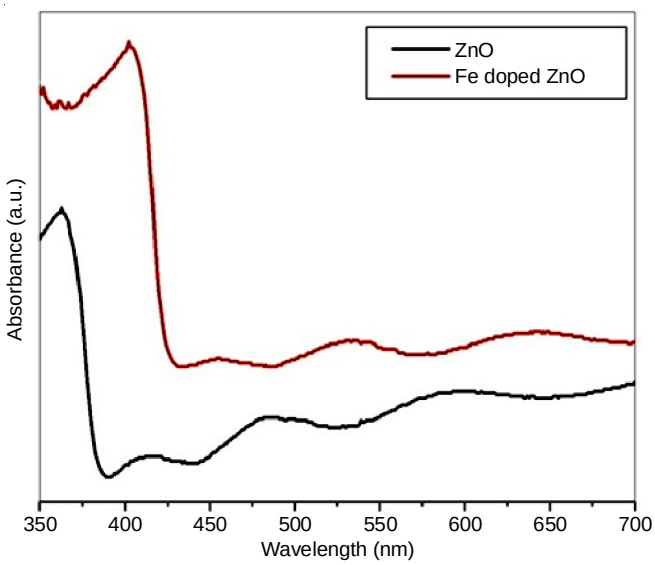

Fig. 3. Absorption *vs*. wavelength curve of ZnO and Fe doped ZnO

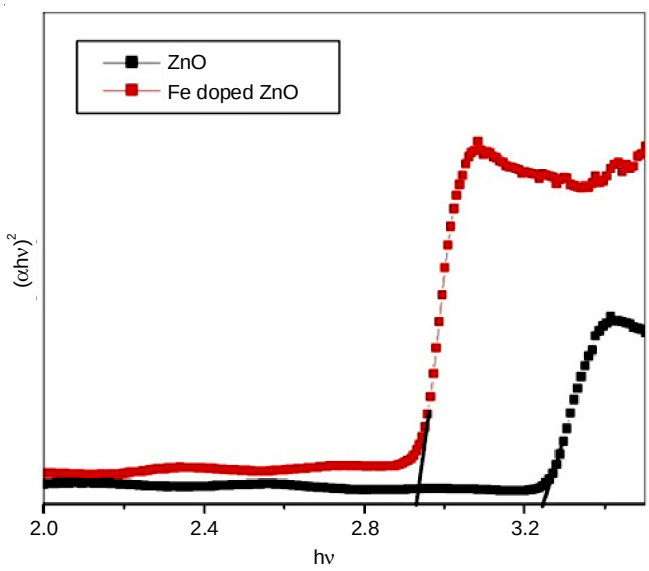

Fig. 4. Plot of $(\alpha h\nu)^2$ *vs*. hν

Fig. 6 shows the SEM images of ZnO and Fe-ZnO thin films. Uniform distribution of the film over the substrate with no major structural defects can be seen. The particle size also reduced in Fe-ZnO thin films.

Resistance *vs*. working temperature: The electrical properties of ZnO and Fe-ZnO were recorded in air as well as in the presence of CO. At room temperature, the resistance was very high and was not measurable. Therefore, resistance was recorded in the range 100-600 °C at the regular increment of 50 °C. At higher temperature due to thermal activation of charge carrier, resistance decreases [16]. The high resistance at room temperature may be due to adsorbed water on the ZnO film which may cause the formation of hydroxyls on the ZnO surface and form a positively charged depletion layer [4]. At higher temperature, desorption of hydroxyl ion takes place and resistance decreases. It is well reported that the sensing response depends on operating temperature. So we investigated sensor response at different operating temperature.

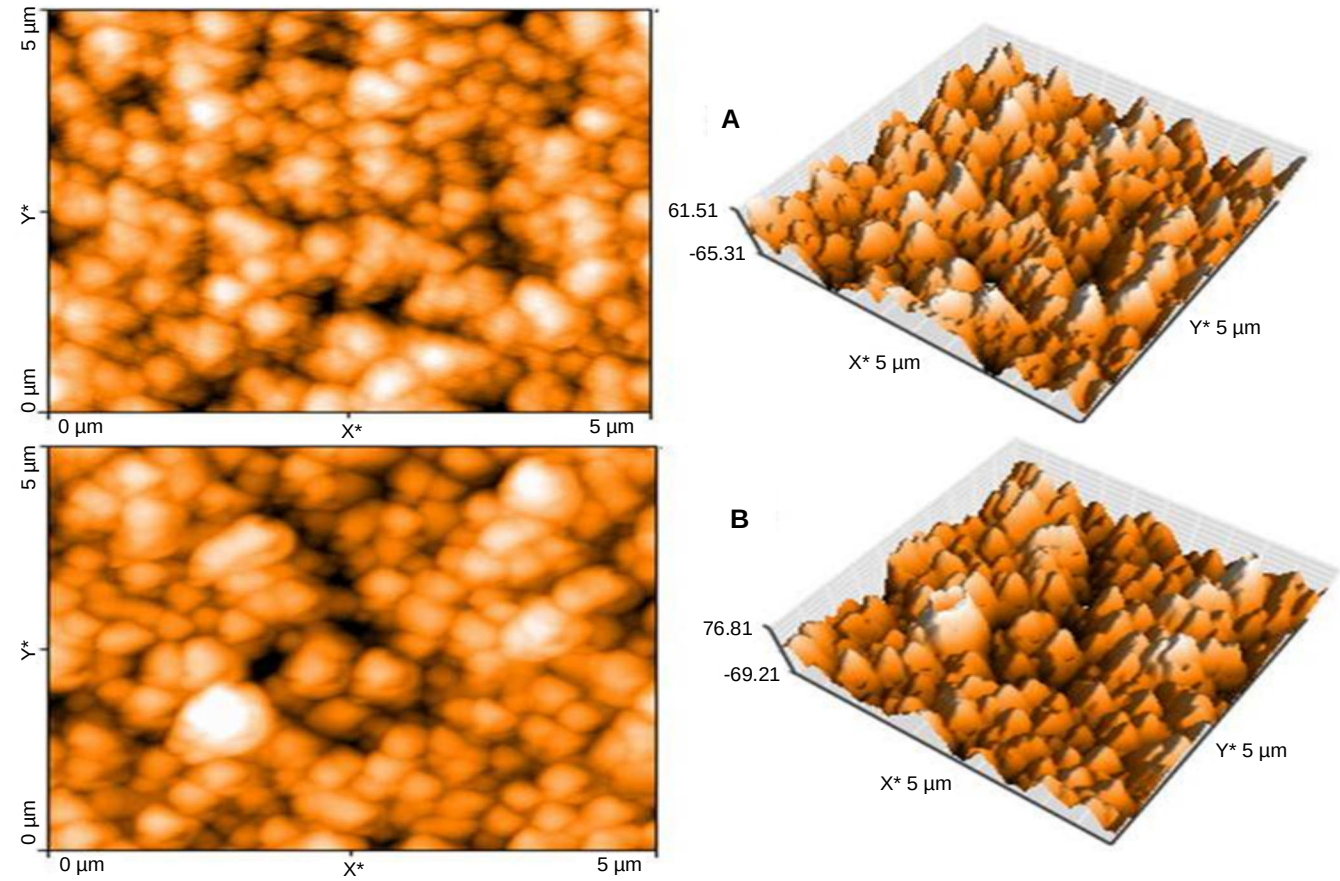

Fig. 5. AFM images of ZnO thin film (A) and Fe doped ZnO (B)

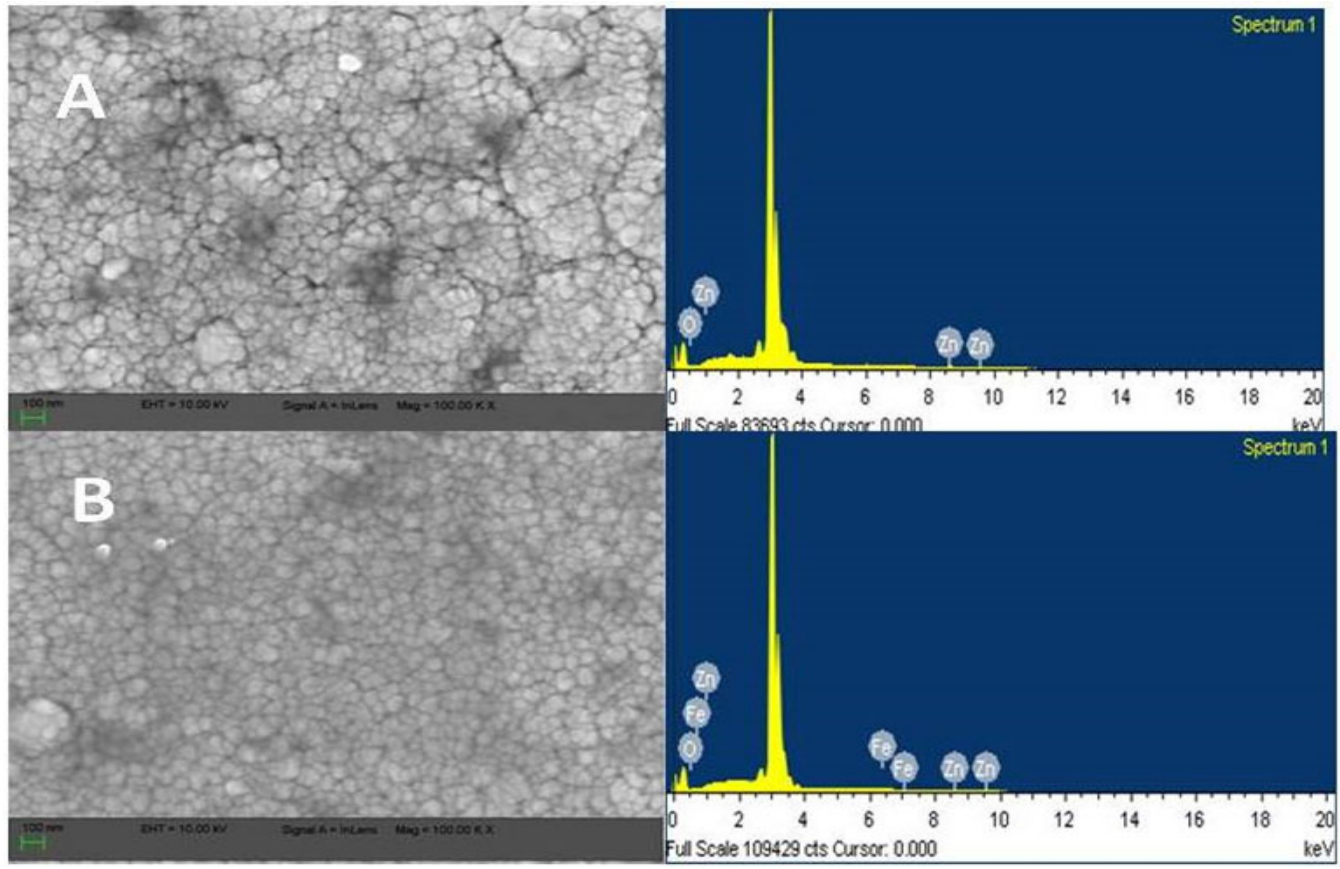

Fig. 6. SEM images of ZnO (A) and Fe doped ZnO (B)

It was observed that ZnO as well as Fe-ZnO were highly sensitive to CO. Both the films offered high resistance in air while in the presence of CO, rapid fall in resistance was recorded (Fig. 7). This shows that films are highly sensitive to the CO gas. On increasing the temperature, the CO molecules which are adsorbed over the surface become more active to react with surface adsorbed oxygen species. The adsorbed CO molecules react with oxygen and produce CO_2 alongwith one electron [17]. The reducing gas CO gets oxidized to CO_2 with liberation of free electron reducing the resistance. In many studies it is reported that resistivity deceases with increase in operating temperature but after certain temperature it again increases [18]. The response depends upon the balance between adsorption and desorption. At higher temperature, desorption takes place which lead to the increase in resistance. Up to 400 °C, the resistance decreases with increase in operating temperature but beyond that it gets saturated and starts to increase with further increase in temperature.

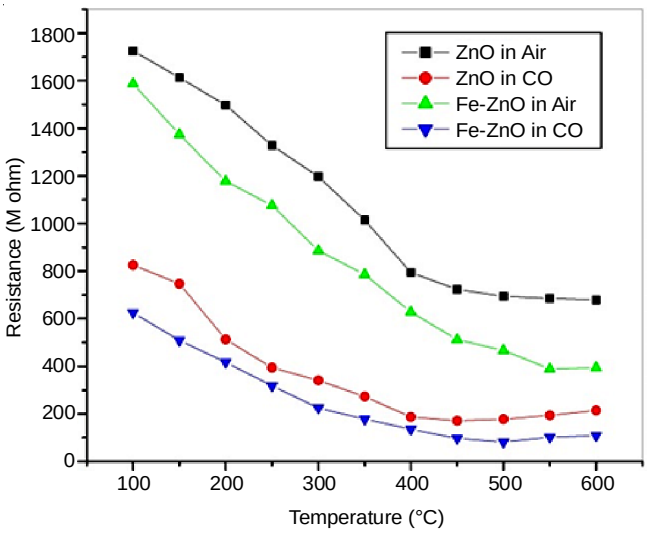

Fig. 7. Resistance *vs.* working temperature curve recorded by using ZnO and Fe-ZnO

Fig. 8 shows the response of ZnO and Fe-ZnO thin films with respect to CO. It was observed that as the operating temperature was increased, sensor response was also increased in both the cases. However, after certain temperature, response of sensor decreased. In case of ZnO, the response decreased above 400 °C while in Fe-ZnO, response started to decrease after 500 °C. This decrease in sensor response may be attributed to desorption of CO gas at higher temperature. To make a balance between adsorption and desorption of gas and to record maximum response, the operating temperature must be optimized [18].

For both ZnO and Fe-ZnO, the introduction of CO leads decrease in resistance which show n-type nature of ZnO was maintained during Fe doping. Compared to ZnO, Fe-ZnO offered less resistance which may be due to the presence of Fe in ZnO matrix. It is reported that Fe exists in the form of Fe^{2+} and Fe^{3+} by mutual exchange of electrons and due to this movement of electrons, resistance decreases. Sensor based on Fe-ZnO show sharp decrease in resistance in presence of CO compared to ZnO which show that on Fe doping the sensitivity of Fe-ZnO sensor increased.

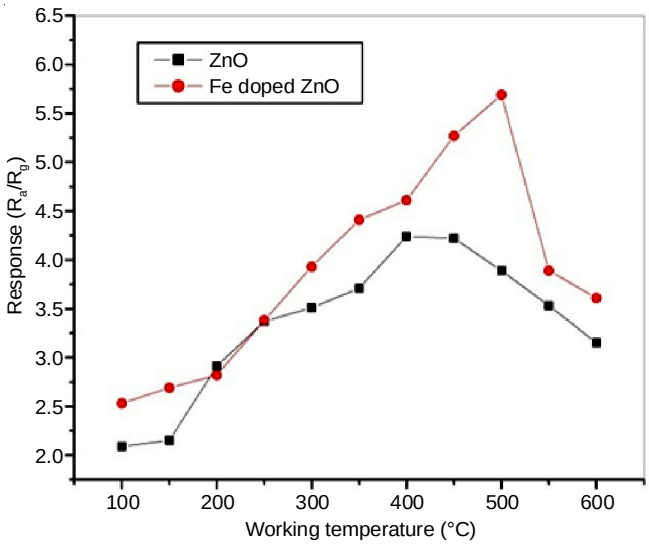

Fig. 8. Response *vs.* working temperature curve recorded by using ZnO and Fe-ZnO

To investigate the sensitivity of ZnO and Fe-ZnO based sensor, the response time and recovery time was also recorded at 150 °C (Fig. 9). The response time of ZnO was 4.76 seconds while that of Fe-ZnO was 3.26 seconds which shows that Fe-ZnO was more sensitive to CO gas. This can be attributed to high electrical conductivity of Fe-ZnO thin films. Carbon monoxide gas gets converted into CO_2 followed by the generation of one electron which decreases the resistance of the films and if the electrical conductivity of the sensing material is good, the resistance decreases rapidly. Recovery time which is one of the most important parameters was also recorded for both ZnO and Fe-ZnO. The recovery time of ZnO based sensor was 39 seconds while that of Fe-ZnO was about 10 seconds. So on the basis of sensing transient curve, high sensitivity of Fe-ZnO based sensors may be concluded.

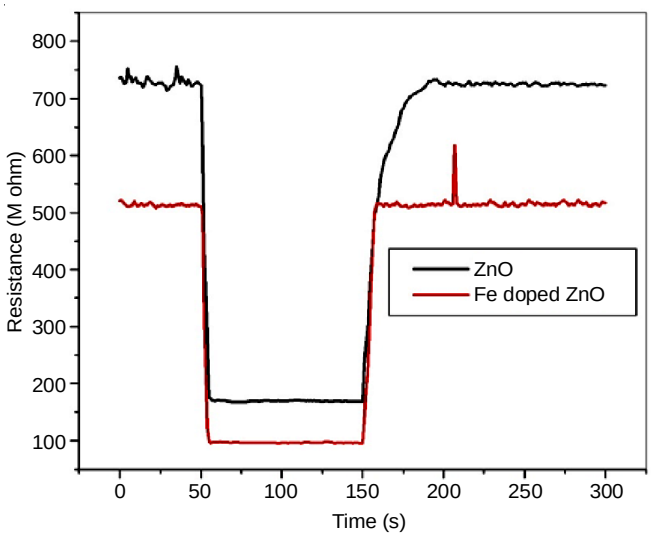

Fig. 9. Resistance *vs.* working temperature curve recorded by using ZnO and Fe-ZnO

Alongwith sensitivity, stability also plays a key role. To check the stability of sensors repeated measurements were also recorded for 40 days. After each measurement, the sensors

were placed in desigator. Fig. 10 shows the response of Fe-ZnO over the days at 450 °C. There is no remarkable change in the response was recorded.

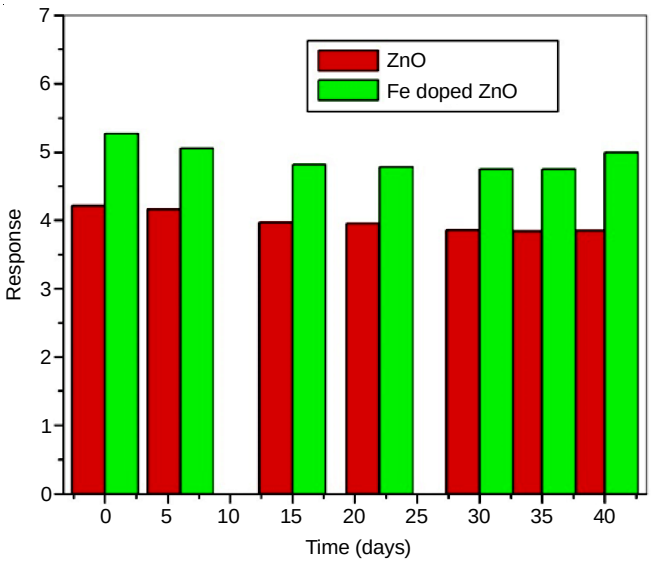

Fig. 10. Response of ZnO and Fe-ZnO based sensors recorded over the days

Conclusion

Zinc oxide and Fe doped ZnO thin films were fabricated on conducting glass by using spin-coating method. Exhaustive evolution of hexagonal wurtzite phase was observed. As synthesized films were used as sensor to sense CO gas. The sensitivity of ZnO thin film was good which increased significantly on Fe doping. Compared to ZnO, Fe doped ZnO thin film offered high gas response. The sensor response was found to be the dependent on operating temperature and was maximum at particular temperature. The study shows that Fe doped ZnO can serve as highly sensitive and stable sensor for CO gas.

ACKNOWLEDGEMENTS

The authors thank Prof. Sahab Dass and Dr. Rohit Shrivastav, Department of Chemistry, Dayalbagh Educational Institute, Agra, India for their generous help in the characterization of samples.

CONFLICT OF INTEREST

The authors declare that there is no conflict of interests regarding the publication of this article.

REFERENCES

1. P.I. Gouma, M. Stanacevic and S. Simon, *Translat. Mater. Res.*, **2**, 045001 (2015); https://doi.org/10.1088/2053-1613/2/4/045001.
2. A. Wei, C.X. Xu, X.W. Sun, W. Huang and G.Q. Lo, *J. Dispers. Technol.*, **4**, 9 (2008); https://doi.org/10.1109/JDT.2007.901569.
3. A. Wei, L. Pan and W. Huang, *Mater. Sci. Eng. B*, **176**, 1409 (2011); https://doi.org/10.1016/j.mseb.2011.09.005.
4. A. Umar, J.-H. Lee, R. Kumar and O. Al-Dossary, *Nanosci. Nanotechnol. Lett.*, **8**, 241 (2016); https://doi.org/10.1166/nnl.2016.2109.
5. S.B. Jagadale, V.L. Patil, S.A. Vanalakar, P.S. Patil and H.P. Deshmukh, *Ceram. Int.*, **44**, 3333 (2018); https://doi.org/10.1016/j.ceramint.2017.11.116.
6. T. Wang, X. Kou, L. Zhao, P. Sun, C. Liu, Y. Wang, K. Shimanoe, N. Yamazoe and G. Lu, *Sens. Actuators B Chem.*, **250**, 692 (2017); https://doi.org/10.1016/j.snb.2017.04.099.
7. B. Santara, B. Pal and P.K. Giri, *J. Appl. Phys*., **110**, 114322 (2011); https://doi.org/10.1063/1.3665883.
8. Z. Qiang, S.Y. Ma, H.Y. Jiao, W.X. Jin, T.T. Wang, X.H. Jiang and Z.Y. Zhang, *Mater. Lett.*, **181**, 29 (2016); https://doi.org/10.1016/j.matlet.2016.06.004.
9. Q. Zhang, C.S. Dandeneau, X. Zhou and G. Cao, *Adv. Mater.*, **21**, 4087 (2009); https://doi.org/10.1002/adma.200803827.
10. L. Znaidi, G.J.A.A. Soler Illia, S. Benyahia, C. Sanchez and A.V. Kanaev, *Thin Solid Films*, **428**, 257 (2003); https://doi.org/10.1016/S0040-6090(02)01219-1.
11. A.H. Nobari and M. Halali, *Chem. Eng. J.*, **121**, 79 (2006); https://doi.org/10.1016/j.cej.2006.05.008.
12. T.M. Hammad, S. Griesing, M. Wotocek, S. Kuhn, R. Hempelmann, U. Hartmann and J.K. Salem, *Int. J. Nanoparticles*, **6**, 324 (2013); https://doi.org/10.1504/IJNP.2013.057175.
13. D. Shuang, X.X. Zhu, J.B. Wang, X.L. Zhong, G.J. Huang and C. He, *Appl. Surf. Sci.*, **257**, 6085 (2011); https://doi.org/10.1016/j.apsusc.2011.02.001.
14. X. Wu, Z. Wei, L. Zhang, X. Wang, H. Yang and J. Jiang, *J. Nanomater.*, **Article ID 792102** (2014); https://doi.org/10.1155/2014/792102.
15. A. Polyakov, A.V. Govorkov, N.B. Smirnov, N.V. Pashkova, S.J. Pearton, K. Ip, R.M. Frazier, C.R. Abernathy, D.P. Norton, J.M. Zavada and R.G. Wilson, *Mater. Sci. Semicond. Process.*, **7**, 77 (2004); https://doi.org/10.1016/j.mssp.2004.03.001.
16. T. Krishnakumar, R. Jayaprakash, N. Pinna, N. Donato, A. Bonavita, G. Micali and G. Neri, *Sens. Actuators B Chem.*, **143**, 198 (2009); https://doi.org/10.1016/j.snb.2009.09.039.
17. J.X. Wang, X.W. Sun, H. Huang, Y.C. Lee, O.K. Tan, M.B. Yu, G.Q. Lo and D.L. Kwong, *Appl. Phys., A Mater. Sci. Process.*, **88**, 611 (2007); https://doi.org/10.1007/s00339-007-4076-8.
18. M. Hjiri, L. El Mir, S.G. Leonardi, A. Pistone, L. Mavilia and G. Neri, *Sens. Actuators B Chem.*, **196**, 413 (2014); https://doi.org/10.1016/j.snb.2014.01.068.